1	Classification:
2	BIOLOGICAL SCIENCES: Cell Biology
3	
4	Ras Inhibitor CAPRI Enables Neutrophils to Chemotax Through a Higher-Concentration
5	Range of Gradients
6	
7	Xuehua Xu <sup>1</sup> , Xi Wen, Amer Moosa, Smit Bhimani, and Tian Jin
8	
9	Chemotaxis Signaling Section, Laboratory of Immunogenetics, National Institute of Allergy and
10	Infectious Diseases, National Institutes of Health, 5625 Fishers Lane, Rockville, MD 20852,
11	USA.
12	
13	<sup>1</sup> To whom correspondence may be addressed. Email: <u>xxu@niaid.nih.gov</u>
14	
15	Key Words:
16	Chemotaxis, neutrophils, G protein-coupled receptor (GPCR), adaptation, Ras, Ras guanine
17	nucleotide exchange factor (Ras GEF), Ras GTPase-activating proteins (RasGAPs), polarity,
18	directional cell migration.
19	
20	Author contributions: X.X. designed research; X.X., X.W., A.M., and S.B. performed research
21	and analyzed data; X.X. and T.J. wrote the paper.
	1   Page

#### 22

23 The authors declare no competing interest.

#### 24 Abstract

- 25 Neutrophils sense and migrate through an enormous range of chemoattractant gradients through
- 26 adaptation. Here, we reveal that, in human neutrophils, Calcium-promoted Ras inactivator
- 27 (CAPRI) locally controls the GPCR-stimulated Ras adaptation. Human neutrophils lacking
- 28 CAPRI (*capri<sup>kd</sup>*) exhibit chemoattractant-induced non-adaptive Ras activation; significantly
- increased phosphorylation of AKT, GSK $3\alpha/3\beta$ , and cofilin; and excessive actin polymerization.
- $capri^{kd}$  cells display defective chemotaxis in response to high-concentration gradients but exhibit
- 31 improved chemotaxis in low- or subsensitive-concentration gradients of various chemoattractants
- 32 as a result of their enhanced sensitivity. Taken together, our data reveal that CAPRI controls
- 33 GPCR activation-mediated Ras adaptation and lowers the sensitivity of human neutrophils so
- that they are able to chemotax through a higher concentration range of chemoattractant gradients.

# 35 Significance Statement

36	Neutrophils provide first-line host defense by migrating through chemoattractant gradients to the
37	sites of inflammation. Inappropriate recruitment and mis-regulated activation of neutrophils
38	contribute to tissue damage and cause autoimmune and inflammatory disease. One fascinating
39	feature of chemotactic neutrophils is their ability to migrate through an enormous concentration
40	range of chemoattractant gradients ( $10^{-9} \sim 10^{-5}$ M) through "adaptation," in which cells no longer
41	respond to the present stimuli, but remain sensitive to stronger stimuli. The inhibitory
42	mechanism largely remains elusive, although many molecules of the excitatory signaling
43	pathway have been identified. Our study reveals, for the first time, that the inhibitory component,
44	CAPRI, is essential for both the sensitivity and the GPCR-mediated adaptation of human
45	neutrophils.

# 46 **/body**

# 47 Introduction

48	Neutrophils provide first-line host defense and play pivotal roles in innate and adaptive
49	immunity (1-3). Inappropriate recruitment and dysregulated activation of neutrophils contribute
50	to tissue damage and cause autoimmune and inflammatory diseases (1, 4). Neutrophils sense
51	chemoattractants and migrate to sites of inflammation using G protein-coupled receptors
52	(GPCRs). To accurately navigate through an enormous concentration-range gradient of various
53	chemoattractants ( $10^{-9} \sim 10^{-5}$ M) (Fig. S1), neutrophils employ a mechanism called adaptation, in
54	which they no longer respond to present stimuli but remain sensitive to stronger stimuli.
55	Homogeneous, sustained chemoattractant stimuli trigger transient, adaptive responses in many
56	steps of the GPCR-mediated signaling pathway downstream of heterotrimeric G proteins (5, 6).
57	Adaptation provides a fundamental strategy for eukaryotic cell chemotaxis through large
58	concentration-range gradients of chemoattractants. Abstract models and computational
59	simulations have proposed mechanisms generating the temporal dynamics of adaptation: an
60	increase in receptor occupancy activates two antagonistic signaling processes, namely, a rapid
61	"excitation" that triggers cellular responses and a temporally delayed "inhibition" that terminates
62	the responses and results in adaptation (5, 7-13). Many excitatory components have been
63	identified during last two decades; however, the inhibitor(s) have just begun to be revealed (11,
64	14-17). It has been recently shown that an elevated Ras activity increases the sensitivity and
65	changes migration behavior (18, 19). However, the molecular connection between the GPCR-
66	mediated adaptation and the cell sensitivity remains missing.
67	The small GTPase Ras mediates multiple signaling pathways that control directional cell

migration in both neutrophils and *Dictyostelium discoideum* (17, 20-24). In *D. discoideum*, Ras

is the first signal event that displays GPCR-mediated adaptation (20). Ras signaling is mainly 69 regulated through its activator, guanine nucleotide exchange factor (GEF), and its inactivator, 70 71 GTPase-activating proteins (GAP) (16, 17, 25). In D. discoideum, the roles of DdNF1 and an Factin-dependent negative feedback mechanism have been previously reported (14, 17). We have 72 previously demonstrated the involvement of locally recruited inhibitors that act on upstream of 73 74  $PI_3K$  in sensing of chemoattractant gradients (11, 26). Recently, we identified a locally recruited RasGAP protein, C2GAP1, that is essential for F-actin-independent Ras adaptation and long-75 76 range chemotaxis in *Dictyostelium* (16). Active Ras proteins enrich at the leading edge in both D. 77 discoideum cells and neutrophils (17, 27, 28). It has been reported that a RasGEF, RasGRP4, plays a critical role in Ras activation in murine neutrophil chemotaxis (21, 29). However, the 78 79 components involved in the GPCR-mediated deactivation of Ras and their function in neutrophil chemotaxis are still not known. 80 In the present study, we show that CAPRI (a Calcium-promoted Ras inactivator) locally controls 81 82 the GPCR-mediated Ras adaptation in human neutrophils. In response to high-concentration stimuli, cells lacking CAPRI (*capri<sup>kd</sup>*) exhibit non-adaptive Ras activation; significantly 83 increased activation of AKT, GSK $3\alpha/3\beta$ , and cofilin; excessive actin polymerization; and 84 subsequent defective chemotaxis. Unexpectedly, *capri<sup>kd</sup>* cells display enhanced sensitivity 85 toward chemoattractants and an improved chemotaxis in low- or subsensitive-concentration 86 gradients. Taken together, our findings show that CAPRI Functions as an inhibitory component 87 of Ras signaling, plays a critical role in controlling the concentration range of chemoattractant 88 89 sensing, and is important for the proper adaptation during chemotaxis.

90

#### 91 **Results**

5 | Page

92	CAPRI regulates GPCR-mediated Ras adaptation in human neutrophils. Chemoattractants
93	induce robust, transient Ras activation in mammalian neutrophils (21, 30). To identify which
94	RasGAP proteins that deactivate Ras in neutrophils, we examined the expression of potential
95	RasGAPs in mouse and human neutrophils (Fig. S2A) (31, 32). We found that human and mouse
96	neutrophils highly expressed CAPRI, also called RASA4, consistent with previous reports (33-
97	35). The human neutrophil-like (HL60) cell line provides a useful model to study mammalian
98	neutrophils (22, 36). The differentiated HL60 cell also highly expresses CAPRI (Fig. S2B),
99	consistent with a previous report (37), and provides a suitable cell system in which to study
100	CAPRI's function in human neutrophils. We found that chemoattractant fMLP (N-formyl-L-
101	methionyl-L-leucyl-phenylalanine) stimulation promoted the association between CAPRI and N-
102	Ras/Rap1(Fig 1A), suggesting a role of CAPRI in the regulation of chemoattractant-induced Ras
103	and Rap1 signaling. To determine the function of CAPRI, we stably knocked down the
104	expression of <i>capri</i> ( <i>capri</i> <sup>kd</sup> ) in HL60 cells using <i>capri</i> -specific shRNA lentiviral particles (Fig.
105	1 $B$ ). We first biochemically determined the dynamics of fMLP-induced Ras activation in both
106	CTL and $capri^{kd}$ cells using a pull-down assay with a large population of cells (Fig. 1C). In
107	resting <i>capri<sup>kd</sup></i> cells, there was a notably higher level of active Ras, indicating CAPRI's function
108	in regulating basal Ras activity in the cells. In response to 1 $\mu$ M fMLP stimulation, we detected a
109	transient Ras activation followed by a secondary reactivation in CTL cells as previously reported
110	(14, 16, 30), but a significantly stronger, prolonged Ras activation in <i>capri<sup>kd</sup></i> cells (Fig. 1D). We
111	further monitored fMLP-induced Ras activation by visualizing the membrane translocation of a
112	fluorescent active Ras probe, the active Ras binding domain of human Raf1 tagged with RFP
113	(RBD-RFP, red), in single live cells using fluorescence microscopy (Fig. 1 <i>E</i> ). In the present
114	study, we used three plasma membrane (PM) markers, Mem-cerulean, C1AC1A-YFP, and
	6   Page

**6 |** P a g e

CAAX-mCherry, to track the cell membrane in live cell experiment (Fig. S3). We monitored Ras 115 activation in CTL and *capri<sup>kd</sup>* cells expressing both PM marker (green) and active Ras probe 116 RBD-RFP (red) in response to uniformly applied 1 µM fMLP stimulation. We found that RBD-117 RFP translocated to and colocalized with PM marker (green) and then returned to the cytoplasm, 118 119 followed by a second translocation to the protrusion sites of CTL cells (Fig. 1E, upper panel, and see Video S1 for a complete, longer time period). In *capri<sup>kd</sup>* cells, the same fMLP stimulation 120 121 induced persistent membrane translocation and accumulation on the continuously expanding and 122 broadened leading front of the cell (Fig. 1E, middle panel, and Video S2). To further examine 123 CAPRI's function in Ras deactivation, we expressed CAPRI-tagged turboGFP (CAPRI-tGFP), RBD-RFP, and PM marker (Mem-cerulean) in *caprikd* cells (*caprikd*/OE) and monitored fMLP-124 induced Ras activation in these cells. 1  $\mu$ M fMLP stimulation triggered a clear membrane 125 126 translocation of CAPRI-tGFP but much weaker or no membrane translocation of RBD-RFP in *capri*<sup>kd</sup>/OE cells (Fig. 1*E*, lower panel, Fig. S4, and Video S3), suggesting that CAPRI 127 128 translocates to the plasma membrane to inhibit Ras activation (33). Quantitative measurement of RBD-RFP membrane translocation confirmed that fMLP stimulation induced a biphasic Ras 129 activation in CTL cells as previously reported (30), a prolonged Ras activation in *capri<sup>kd</sup>* cells, 130 and a reduced Ras activation in  $capri^{kd/OE}$  cells (Fig. 1F). Taken together, our results indicate 131 that CAPRI is a RasGAP protein and is required for chemoattractant-mediated Ras adaptation in 132 neutrophils. 133

134

Membrane targeting of CAPRI in response to chemoattractant stimulation. To reveal how
 CAPRI functions during neutrophil chemotaxis, we examined cellular localization of CAPRI tGFP in HL60 cells. We found that CAPRI-tGFP colocalized with active Ras (RBD-RFP) and
 7 | P a g e

actin at the leading edge of chemotaxing HL60 cells in a fMLP gradient (Fig. 2A), consistent 138 with previous reports (16, 22, 35). Chemoattractant fMLP and IL-8 induced membrane 139 translocation of CAPRI-tGFP (Fig. 1E and Fig. S4-S5). The G protein inhibitor pertussis toxin 140 (PT) blocked the membrane translocation of CAPRI (Fig. S6), indicating that chemoattractant 141 GPCR/G protein-mediated signaling is required for CAPRI membrane targeting. To reveal the 142 143 molecular mechanism of CAPRI membrane targeting, we investigated the domain requirement for its membrane translocation and interaction with Ras. We expressed tGFP-tagged WT and 144 145 mutants of  $\Delta C2$ ,  $\Delta PH$ , and a GAP-inactive mutant R472A, and determined their ability for Ras interaction (Fig. 2B-2C and Fig. S7). We found that  $\Delta$ C2 did not interact with Ras and R472A 146 showed a decreased interaction with Ras (Fig. 2C), consistent with previous reports (33, 38-41). 147 148 We next monitored the membrane translocation ability of CAPRI WT and its mutant in response 149 to fMLP stimulation (Fig. 2D). Upon fMLP stimulation, WT and R472A clearly translocated to 150 and colocalized with PM marker (Fig. 2D, top two panels and Video S4-S5), while  $\Delta$ PH and  $\Delta$ C2 showed significantly decreased or little membrane translocation (Fig. 2D, lower two panels, 151 152 and Video S6-S7). Using total internal reflections fluorescent (TIRF) microscopy, we confirmed 153 the membrane-translocation behavior of CAPRI WT and its mutants (Fig. S8 and Fig. 2E) (42). 154 Our results indicate that both the C2 and PH domains are crucial for chemoattractant-induced 155 membrane targeting. 156

157 Chemoattractant induces hyperactivation of Ras effectors in *capri<sup>kd</sup>* cells. PI3Kγ is a direct
 158 effector of Ras, which synthesizes lipid phosphatidylinositol (3,4,5)-trisphosphate

159 (PtdIns $(3,4,5)P_3$ , PIP<sub>3</sub>) and activates the PIP<sub>3</sub>-binding protein AKT in neutrophils (21, 29, 43).

160 To examine the consequence of non-adaptive Ras activation, we monitored fMLP-induced PIP<sub>3</sub>8 | P a g e

161	production using a biosensor PH-GFP (PH-domain of human AKT tagged with GFP, green) in
162	both CTL and <i>capri<sup>kd</sup></i> cells (Fig. 3A) (44). We found that 1 $\mu$ M fMLP trigged a robust
163	translocation of PH-GFP to the entire plasma membrane followed by a partial return to the
164	cytosol and a gradual accumulation in the protrusion site of CTL cell (Fig. 3A, upper panel, and
165	Video S8). The same stimulation induced a stronger and persistent accumulation of PH-GFP all
166	around the periphery of <i>capri<sup>kd</sup></i> cells (Fig. 3A, lower panel, and Video S9), indicating a
167	hyperactivation of PI3K in cells lacking CAPRI. We further determined the activation profile of
168	PI <sub>3</sub> Kγ downstream effectors in CTL and <i>capri<sup>kd</sup></i> cells. AKT and GSK are well-known effectors of
169	Ras/PI3Ky signaling and are critical for the reorganization of actin cytoskeleton in neutrophil
170	chemotaxis (22, 45). Therefore, we examined fMLP-induced PI3Ky activation by measuring the
171	phosphorylation of AKT on residues T308 and T473 in both CTL and <i>capri<sup>kd</sup></i> cells. We found
172	that 1 $\mu$ M fMLP triggered a transient phosphorylation on T308 and T473 of AKT in CTL cells,
173	while it induced a persistent and significantly increased phosphorylation on both residues of
174	AKT in <i>capri<sup>kd</sup></i> cells (Fig. 3 <i>B</i> -3 <i>C</i> ), consistent with previous reports (46-48). Cofilin, an F-actin
175	depolymerization factor (ADF), is essential for depolymerization of F-actin in dynamic
176	reorganization of the actin cytoskeleton during cell migration (49). Its activity is regulated
177	mainly through a phosphorylation event: phosphorylation on Ser-3 inhibits its actin binding,
178	severing, and depolymerizing activities; and dephosphorylation on Ser-3 by slingshot proteins
179	(SSHs) reactivates it. Slingshot 2 is a direct substrate of GSK3 and chemoattractants induce
180	phosphorylation and inhibition of GSK3 $\alpha/3\beta$ partially through PI3K $\gamma$ -AKT pathways in
181	neutrophils (45). As previously reported (45), GSK3 $\alpha/3\beta$ is constitutively active and
182	dephosphorylated in resting cells, and fMLP induced a transient phosphorylation and

183	deactivation of GSK3 $\alpha/3\beta$ and led to a transient dephosphorylation of cofilin (Fig. 3D-3E). We
184	found that 1 $\mu$ M fMLP stimulation triggered significantly stronger, prolonged phosphorylation of
185	GSK3 $\alpha/3\beta$ and persistent dephosphorylation of cofilin in <i>capri<sup>kd</sup></i> cells. Taken together, these
186	results indicate that CAPRI is essential for the proper activation/deactivation dynamics of the
187	PI3Ky/AKT/GSK3/cofilin signaling pathway in response to chemoattractant stimulations.

188

fMLP stimulation induces an increased activation of Rap1 and its effector in *caprikd* cells. 189 Rap1 is a close relative of Ras initially described as a competitor of Ras by directly interacting 190 with Ras effectors (50, 51). Later studies indicate that Rap1 also functions in independent 191 192 signaling pathways to control diverse processes, such as cell adhesion, cell-cell junction formation, and cell polarity (52, 53). It has been shown that CAPRI also interacts with Rap1 in 193 194 CHO cells (54). We found that fMLP stimulation promoted the interaction between CAPRI and 195 Rap1 in neutrophils (Fig. 1A) and that CAPRI was recruited to adhesion sites and colocalized with the PM marker during cell migration (Fig. S9). To understand CAPRI's function in Rap1 196 activation in human neutrophils, we determined fMLP-induced Rap1 activation in both CTL and 197 198 capri<sup>kd</sup> cells by a pull-down assay using the Rap-GTP binding domain of human RalGDS (RBD<sub>RalGDS</sub>) (Fig. 4A). There was a higher level of active Rap1 in resting *capri<sup>kd</sup>* cells. fMLP 199 200 stimulation (1 µM) induced a transient Rap1 activation in CTL cells, while it triggered a significantly increased and prolonged Rap1 activation in  $capri^{kd}$  cells (Fig. 4B). We further 201 202 monitored Rap1 activation using an active Rap1 probe, GFP-tagged RBD<sub>RalGDS</sub> (RBD<sub>RalGDS</sub>-GFP) (52), using live cell fluorescence microscopy (Fig. 4C). We found that RBD<sub>RalGDS</sub>-GFP 203 colocalized with PM marker at the adhesion/protrusion sites of the resting cells (Fig. 4C), 204

suggesting a potential function of Rap1 in the adhesion of neutrophils. Upon 1 µM fMLP 205 206 stimulation, RBD<sub>RalGDS</sub>-GFP (green) transiently translocated to and colocalized with PM marker (red), then returned to the cytoplasm, and then translocated to and colocalized with the PM 207 208 marker again at the protruding sites of CTL cells (Fig. 4C, upper panel, and Video S10). In resting *capri<sup>kd</sup>* cells, there was notably more membrane localization of RBD<sub>RalGDS</sub>-GFP, which is 209 consistent with the notion that there is a higher basal Rap1 activity in  $capri^{kd}$  cells (Fig. 4C, 210 lower panel). We further found that 1 µM fMLP triggered prolonged translocation of RBD<sub>RalGDS</sub>-211 GFP (green) to and colocalization with the PM marker (red) during a continuous expansion of 212 *caprikd* cells (Video S11), suggesting that the fMLP induces a hyperactivation of Rap1 in cells 213 lacking CAPRI. To understand the effects of Rap1 hyperactivation, we examined Rap1 effector 214 Erk42/44 phosphorylation (Fig. 4D). We detected higher basal Erk42/44 phosphorylation in the 215 non-stimulated *capri<sup>kd</sup>* cells. In contrast to a rapid maximum phosphorylation of Erk 42/44 at 30 216 217 s in CTL cells, same stimulation induced an increasing dynamics of Erk42/44 phosphorylation in *capri<sup>kd</sup>* cells (Fig. 4*E*), consistent with previous reports (33, 35, 54). Our results suggest that 218 CAPRI deactivates Rap1 activation to facilitate an appropriate Rap1 activation and its effector 219 220 for chemotaxis in neutrophils.

# Excessive polymerization of actin impairs the polarization and migration of *capri<sup>kd</sup>* cells. The chemoattractant GPCR/G-protein signaling regulates spatiotemporal activities of Ras and Rap1 that mediate multiple signaling pathways to control the dynamics of actin cytoskeleton that drives cell migration. To evaluate the role of CAPRI in chemoattractant GPCR-mediated actin assembly in neutrophils, we determined fMLP-mediated polymerization of actin in CTL and *capri<sup>kd</sup>* cells using a centrifugation assay of actin filaments (F-actin) (Fig. 5A). In CTL cells, 10

µM fMLP stimulation induced a transient polymerization of actin. In *capri<sup>kd</sup>* cells, the same 227 228 stimulation also triggered the initial, transient actin polymerization followed by a much stronger and persistent actin polymerization (Fig. 5A-5B). To understand the temporospatial dynamics of 229 230 actin polymerization, we next monitored actin polymerization using the membrane translocation 231 of an actin filament probe, F-tractin-GFP, in live cells by fluorescence microscopy (55). We found that, in response to uniformly applied 1 µM fMLP, F-tractin-GFP (green) translocated to 232 and colocalized with the PM marker (red) along the entire periphery of CTL cells, then 233 withdrew, and accumulated at the protruding sites of CTL cells (Fig. 5C, upper panel and Video 234 235 S12), indicating an initial overall actin polymerization on the entire periphery followed by a localized polymerization on the protrusion sites. In *capri<sup>kd</sup>* cells, the same stimulation trigged a 236 stronger and prolonged membrane translocation of F-tractin-GFP, followed by a slight 237 238 withdrawal, and then continuous accumulation on multiple expending/ruffling sites of cells (Fig. 239 5C, lower panel and Video S13). To understand the effect of excessive actin polymerization on 240 chemotaxis, we visualized the distribution of F-actin in cells migrating toward a 1 µM fMLP gradient using another F-actin probe (SiR-actin, a live-cell staining probe) (Fig. 5D). As 241 242 expected, CTL cells displayed a clearly polarized actin polymerization: a protruding leading front (pseudopod) and a contracting trailing edge (uropod), and they chemotaxed through the 243 244 gradient and accumulated at the source of the fMLP gradient (Fig. 5D, left panel and Video S14). However, the *capri<sup>kd</sup>* cells, especially those close to the source of the 1 µM fMLP gradient, 245 displayed an overall excessive F-actin distribution, poor polarization, and significantly slow 246 migration during chemotaxis (Fig. 5D, right panel and Video S15). Notably, some of the *capri<sup>kd</sup>* 247 cells located relatively far away from the source of fMLP showed polarized morphology and 248 249 migrated effectively toward the fMLP source, but gradually lost their polarity and stopped 12 | Page

moving when they were close to the source of the fMLP (Video S15). The above results together indicate that chemoattractant stimuli at high concentrations induce excessive polymerization of actin that impairs the polarization and migration of  $capri^{kd}$  cells.

253 *caprikd* cells display improved chemotaxis in low- or subsensitive-concentration gradients of

254 chemoattractants, but defective chemotaxis in high-concentration gradients. To further

determine the function of CAPRI in chemotaxis of neutrophils, we monitored chemotaxis

behavior of CTL and *capri<sup>kd</sup>* cells in gradients of fMLP at different concentrations using an *EZ*-

257 *TAXIScan* analysis (56). In a 1 μM fMLP gradient, *capri<sup>kd</sup>* cells, in a clear contrast to CTL cells,

displayed a significant decrease in migrating speed (CTL:  $20.86 \pm 3.12 \,\mu$ m/min; *caprikd*: 12.16

 $\pm$  3.73 µm/min), directionality (CTL: 0.86  $\pm$  0.09; *caprikd*: 0.73  $\pm$  0.14 µm/min), total path

length (CTL: 140.56  $\pm$  27. 7  $\mu$ m; *caprikd*: 86.74  $\pm$  13.75  $\mu$ m), and polarity measured as

roundness of a cell (%) (CTL:  $76.2 \pm 6.81$ ; *caprikd*:  $84.82 \pm 5.76$ ) (Fig. 6A-6B). To understand

chemotaxis behavior over a large concentration range, we further monitored the chemotaxis

behavior of both CTL and  $capri^{kd}$  cells in the fMLP gradients at lower concentrations (Fig. 6*C*).

264 We found that severe defects in chemotaxis in  $capri^{kd}$  cells were clearly observed when they

experienced fMLP gradients at high concentration (>100 nM). When exposed to a gradient

266 generated from a lower concentration (10 nM fMLP source, both CTL and *capri<sup>kd</sup>* cells displayed

similar directionality, although *capri<sup>kd</sup>* cells still displayed decreased speed and total path length

268 (Fig. 6*D*). In response to a gradient generated from a 1 nM fMLP source,  $capri^{kd}$  cells displayed

significantly better directionality, but similar migration speed, in comparison with CTL cells. In

- a 0.1 nM fMLP gradient, most CTL cells displayed random migration, while the majority of
- 271 *capri<sup>kd</sup>* cells displayed improved directionality and migration speed. Without a gradient, *capri<sup>kd</sup>*

cells displayed a bigger random walk compared to CTL cells. That is, *capri<sup>kd</sup>* cells display defective chemotaxis in high-concentration gradients but improved chemotaxis in low- or subsensitive-concentration gradients of chemoattractants. We also observed this concentrationdependent change of chemotaxis capability of *capri<sup>kd</sup>* cells in response to gradients of IL-8, another chemoattractant for neutrophils (Fig. S10). The above result indicates that CTL cells chemotaxed efficiently through gradients of various chemoattractants ranging from  $10^{-9}$  to  $10^{-6}$ M, while *capri<sup>kd</sup>* cells did so from  $10^{-10}$  to  $10^{-7}$  M.

An increased sensitivity of *capri<sup>kd</sup>* cells toward chemoattractants. Using TIRF imaging, we 279 noticed that CAPRI-tGFP localized on the membrane of resting cells, suggesting its potential 280 281 role in inhibiting basal Ras activity (Fig. 7A). As expected, fMLP stimulation induced a strong, quick membrane translocation of CAPRI followed by a slow, gradual withdrawal with a notable 282 fraction of CAPRI remaining on the plasma membrane for quite a long period of time. We also 283 observed a higher basal Ras activity in  $capri^{kd}$  cells (Fig. 1C), indicating a potential role of 284 CAPRI in maintaining a low basal Ras activity in the resting cells. The basal activity of Ras is 285 part of a positive feedback mechanism that promotes actin dynamics and, more importantly, 286 chemotaxis in a shallow chemoattractant gradient in D. discoideum (24). We speculated that the 287 higher basal Ras activity in *capri<sup>kd</sup>* cells might contribute to their enhanced random walk without 288 289 a gradient or to their improved chemotaxis in a low- or subsensitive-concentration gradient (Fig. 6). To determine whether  $capri^{kd}$  cells have become more sensitive to the stimulus, we 290 determined Ras and Rap1 activation in response to fMLP stimulation at different concentrations 291 using a pull-down assay (Fig. 7B). Comparing to the CTL cells, we detected a stronger Ras/Rap1 292 activation in *capri<sup>kd</sup>* cells in response to all three different concentrations (Fig. 7*C*). In response 293 to 0.1 nM fMLP stimulation, CTL cells did not show a clear Ras or Rap1 activation but 294 **14** | Page

displayed a weak oscillation, while  $capri^{kd}$  cells showed a clear transient Ras activation. In response to 10 nM and 1  $\mu$ M fMLP stimulation,  $capri^{kd}$  cells showed a stronger, longer activation of both Ras and Rap1 than CTL cells did.

We further determined the responsiveness of both CTL and *capri<sup>kd</sup>* cells to either 0.1 nM or 10 298 nM fMLP stimulation by monitoring actin polymerization through the membrane translocation 299 300 of F-tractin-GFP (Fig. 8). In response to 0.1 nM fMLP stimulation, most CTL cells (~ 90 %) did not show clear membrane translocation of F-tractin-GFP to the plasma membrane, while they 301 showed a continuous translocation of F-tractin-GFP to the protrusion sites (Fig. 8A, top panel, 302 and Video S16). In contrast, more than 80 % of the *capri<sup>kd</sup>* cells showed clear membrane 303 translocation of F-tractin upon 0.1 nM fMLP stimulation (Video S17 and Fig. 8B), indicating a 304 higher sensitivity of *capri<sup>kd</sup>* cells. Not surprisingly, 10 nM fMLP induced robust membrane 305 translocation of F-tractin in both CTL and *capri<sup>kd</sup>* cells with different dynamics: CTL cells 306 showed a clear transient translocation of F-tractin-GFP to plasma membrane (~ 5-40 s), followed 307 308 by a withdrawal of most F-tractin from the plasma membrane (~ 50-60 s) and then a second translocation to the protrusion sites (> 60 s) (Video S18); while *capri<sup>kd</sup>* cells showed a stronger 309 and longer membrane translocation of F-tractin-GFP to plasma membrane (~ 5-90 s) followed by 310 311 a gradual withdrawal (~ 90-130 s) (Video S19), indicating a stronger response and a longer period of time required to adapt the stimulation. Consistent with the results above, a prolonged, 312 non-adaptive actin polymerization was observed in *caprikd* cells in response to stimuli at higher 313 concentrations (Fig. 5 and Fig. 8*C*). These results together demonstrate that  $capri^{kd}$  cells, lacking 314 Ras inhibitor, are sensitive to subsensitive-concentration chemoattractant stimuli for CTL cells, 315 while they fail to chemotax through a high-concentration gradient as CTL cells do. 316

15 | Page

#### 317 Discussion

Here, we show that CAPRI is a locally membrane-recruited negative regulator of Ras signaling 318 and enables neutrophils to chemotax through a higher concentration range of chemoattractant 319 gradients by lowering their sensitivity and through GPCR-mediated adaptation. 320 Chemoattractant-induced deactivation of Ras is regulated through the local membrane 321 recruitment of CAPRI. The membrane recruitment of CAPRI and its function in Ras 322 deactivation have been previously studied (33, 39). CAPRI, CAlcium-Promoted Ras Inactivator, 323 324 was first characterized by its calcium-dependency on deactivation of Ras (33). In this study, we found that the  $\Delta C2$  mutant of CAPRI did not translocate in response to chemoattractant 325 stimulation, indicating an essential role of C2/calcium binding in the membrane targeting of 326 CAPRI (Fig. 2*E*). In addition to the C2 domain, we found that the  $\Delta$ PH mutant showed 327 significantly decreased membrane translocation in response to chemoattractant stimulation (Fig. 328 329 2D-2E). This result is consistent with the previous reports that the PH domain of the GAP1 330 family is responsible for, or plays an important role, in their membrane translocation (34, 39, 57, 331 58). We also found that deactivation of GAP activity of the GAP domain (R472A mutant) had no effect on CAPRI's membrane targeting (Fig. 2D), although it might affect its interaction with 332 333 Ras (Fig. 2E), consistent with the notion that the arginine residue of the GAP domain not only is responsible for its GAP activity, but also stabilizes its interaction with Ras (41). We also found 334 that *caprikd/OE* cells, which displayed little or no Ras activation, still exhibited a strong CAPRI 335 membrane translocation, indicating that active status of Ras is not required for CAPRI membrane 336 translocation. These results indicate that membrane translocation of CAPRI and its function as a 337 338 GAP protein are sequential and yet independent.

#### 339 Inhibitor for the GPCR-mediated adaptation regulates the sensitivity of a eukaryotic cell.

Motile Escherichia coli (E. coli) provides the simplest and the best understood model of 340 chemosensing system that is also mediated by chemoreceptors (59, 60). Modification of the 341 chemoreceptors and interactions among the chemoreceptors have been proposed for a robust 342 response, a precise adaptation, and a high sensitivity of chemoreceptors in bacteria (61-63). 343 344 However, the molecular mechanism by which to control the GPCR-mediated adaption and the sensitivity of a eukaryotic cell in chemotaxis are not fully understood. A local excitation and 345 346 global inhibition (LEGI) model explained how a eukaryotic cell responds to chemoattractant 347 stimuli with a wide-concentration range, achieves adaptation, and establishes the intracellular polarization (10, 64). Different from E. coli, chemoattractant stimulation induces a persistent 348 activation of heterotrimeric G protein in *Dictyostelium* (6, 11, 26), indicating that adaptation 349 350 occurs downstream of GPCR/G protein in the eukaryotic cell. We constructed a detailed model 351 to explain adaptation and chemosensing of *Dictyostelium* cells (15, 65), which led us to uncover 352 the essential role of Ras inhibitors in the GPCR-mediated adaptation (11, 16). Recently, it has been shown that reducing the  $PI(3,4)P_2$  level on the plasma membrane increases Ras activity and 353 enhances the excitability in D. discoideum (18, 19) and that active Ras plays a role in basal 354 355 locomotion and in chemotaxing through very shallow gradients (24). We also detected a higher basal activity of Ras and Rap1 in *capri<sup>kd</sup>* cells. These reports inspired us to test the chemotaxis 356 capability of both CTL and *capri<sup>kd</sup>* cells using wide concentration-range gradients of various 357 358 chemoattractants (Fig. 6 and Fig. S10). In response to fMLP gradients, CTL cells chemotaxed better than *capri<sup>kd</sup>* cells did in gradients at high concentrations (> 100 nM), while they displayed 359 similar chemotaxis capability to  $capri^{kd}$  cells in mild gradients (10 nM of fMLP). In weak 360 gradients (< 1 nM), *caprikd* cells chemotaxed better than CTL cells did. Similar chemotaxis 361

behavior was also observed when CTL and *capri<sup>kd</sup>* cells were exposing to gradients of IL-8. 362 Interestingly, *capri<sup>kd</sup>* cells sensed and responded to weak gradients of fMLP and IL-8 at the 363 concentration that are subsensitive to CTL cells due to a higher sensitivity of *capri<sup>kd</sup>* cells (Fig. 7 364 and Fig. 8). Thus, our study provides evidence that human neutrophils locally recruits Ras 365 inhibitor, CAPRI, to regulate Ras adaptation and their sensitivity. CAPRI enables human 366 367 neutrophils to chemotax through a higher-concentration range of chemoattractant gradients by lowering its sensitivity and by mediating the GPCR-mediated adaptation. 368 Multiple RasGAP proteins might be involved in Ras deactivation in chemoattractant-369 induced adaptation of neutrophils. In the present study, we have shown that CAPRI mediates 370 371 chemoattractant-induced Ras adaptation and sensitivity of neutrophils. Human neutrophils without CAPRI fail in chemoattractant-induced adaptive Ras activation; have significantly 372 373 increased phosphorylation of AKT, GSK $3\alpha/3\beta$ , and cofilin; demonstrate excessive actin polymerization; and exhibit a subsequent defect in chemotaxis in response to high-concentration 374 375 gradients. However, in response to a low-concentration (either 0.1 nM or 10 nM fMLP) stimulation, *caprikd* cells displayed transient Ras/ Rap1 activation and actin polymerization, 376 377 although they displayed prolonged, non-adaptive responses upon stimulation with higher 378 concentrations (Fig. 1, Fig. 7, and Fig. 8). HL60 cells also expressed RASAL1 and RASAL2 379 (Fig. S2)(37), which also deactivate Ras (34, 39). In mouse and human neutrophils, there are 380 other RasGAP proteins expressed in addition to CAPRI (Fig. S2). p120 GAP is present in both 381 human and mouse neutrophils but absent in HL60 cells (66) and its role has been implicated in cell migration (67, 68). While we revealed a major role of CAPRI in mediating the GPCR-382

383	mediated Ras ada	ptation in HL60 c	cells, it is also c	crucial to determine	potentially	y roles of other
-----	------------------	-------------------	---------------------	----------------------	-------------	------------------

384 RasGAP proteins in Ras adaptation and chemotaxis in primary mammalian neutrophils.

#### 385 Acknowledgements

- We thank Drs. Arjan Kortholt, Xinzhuan Su, and Peter Crompton for their critical reading of the
- article. This work was supported by the NIH Intramural Fund from the National Institute of
- 388 Allergy and Infectious Diseases, National Institutes of Health.

#### 389 Materials and Methods

- 390 Detailed descriptions of cells, cell lines, cell culture, and differentiation, reagents and antibodies,
- 391 plasmids and transfection of cells, immunoblotting of fMLP-mediated signaling components,
- Ras and Rap1 activation assay, actin polymerization assay, immunoprecipitation assay, imaging
- and data processing, TAXIScan chemotaxis assay and data analysis, and SiR-actin staining are in
- 394 Supplementary information.

#### 395 **References**

- 396 1. S. Nourshargh, R. Alon, Leukocyte migration into inflamed tissues. Immunity 41, 694-707 (2014). C. Tecchio, A. Micheletti, M. A. Cassatella, Neutrophil-derived cytokines: facts beyond 397 2. expression. Frontiers in immunology 5, 508 (2014). 398 A. Mantovani, M. A. Cassatella, C. Costantini, S. Jaillon, Neutrophils in the activation and 399 3. 400 regulation of innate and adaptive immunity. Nat Rev Immunol 11, 519-531 (2011). 401 4. E. Kolaczkowska, P. Kubes, Neutrophil recruitment and function in health and inflammation. Nat 402 Rev Immunol 13, 159-175 (2013). 403 O. Hoeller, D. Gong, O. D. Weiner, How to understand and outwit adaptation. Dev Cell 28, 607-5. 404 616 (2014).
- 405 6. C. Janetopoulos, T. Jin, P. Devreotes, Receptor-mediated activation of heterotrimeric G-proteins 406 in living cells. *Science* **291**, 2408-2411 (2001).
- 407 7. P. Devreotes, C. Janetopoulos, Eukaryotic chemotaxis: distinctions between directional sensing
  408 and polarization. *The Journal of biological chemistry* **278**, 20445-20448 (2003).
- 4098.A. R. Houk *et al.*, Membrane tension maintains cell polarity by confining signals to the leading410edge during neutrophil migration. *Cell* **148**, 175-188 (2012).

<ol> <li>A. Nakajima, S. Ishihara, D. Imoto, S. Sawai, Rectified directional sensing in long-range cell migration. <i>Nat Commun</i> 5, 5367 (2014).</li> <li>C. A. Parent, P. N. Devreotes, A cell's sense of direction. <i>Science</i> 284, 765-770 (1999).</li> <li>X. Xu, M. Meier-Schellersheim, J. Yan, T. Jin, Locally controlled inhibitory mechanisms are involved in eukaryotic GPCR-mediated chemosensing. <i>The Journal of cell biology</i> 178, 141-</li> </ol>	153
<ul> <li>413 10. C. A. Parent, P. N. Devreotes, A cell's sense of direction. <i>Science</i> 284, 765-770 (1999).</li> <li>414 11. X. Xu, M. Meier-Schellersheim, J. Yan, T. Jin, Locally controlled inhibitory mechanisms are</li> </ul>	153
414 11. X. Xu, M. Meier-Schellersheim, J. Yan, T. Jin, Locally controlled inhibitory mechanisms are	153
	153
415 IIIVOIVEU III EUKAIVOLIL GEUR-IIIEUIALEU LITETITOSETISITE. TITE JOULIUI OLLETI DIODOUV $1/6$ . 141-	133
416 (2007).	
417 12. K. Takeda <i>et al.</i> , Incoherent feedforward control governs adaptation of activated ras in a 418 eukaryotic chemotaxis pathway. <i>Sci Signal</i> <b>5</b> , ra2 (2012).	
<ul> <li>418 eukaryotic chemotaxis pathway. <i>Sci Signal</i> 5, ra2 (2012).</li> <li>419 13. W. Ma, A. Trusina, H. El-Samad, W. A. Lim, C. Tang, Defining network topologies that can a</li> </ul>	shiovo
419 13. W. Ma, A. Trusina, H. El-samad, W. A. Lim, C. Tang, Defining network topologies that can a 420 biochemical adaptation. <i>Cell</i> <b>138</b> , 760-773 (2009).	Juieve
421 14. P. G. Charest <i>et al.</i> , A Ras signaling complex controls the RasC-TORC2 pathway and directed	
421 14. P. G. Charlest <i>et al.</i> , A kas signaling complex controls the kase-roke2 pathway and directed 422 migration. <i>Dev Cell</i> <b>18</b> , 737-749 (2010).	i cen
423 15. X. Xu <i>et al.</i> , Coupling mechanism of a GPCR and a heterotrimeric G protein during	
423 13. A viet d., coupling mechanism of a Greek and a neterotriment of protein during 424 chemoattractant gradient sensing in Dictyostelium. <i>Sci Signal</i> <b>3</b> , ra71 (2010).	
425 16. X. Xu <i>et al.</i> , GPCR-controlled membrane recruitment of negative regulator C2GAP1 locally	
426 inhibits Ras signaling for adaptation and long-range chemotaxis. <i>Proc Natl Acad Sci U S A</i> <b>1</b>	i /i
427 E10092-E10101 (2017).	L <b>-</b> ,
428 17. S. Zhang, P. G. Charest, R. A. Firtel, Spatiotemporal regulation of Ras activity provides direc	tional
429 sensing. <i>Current biology : CB</i> <b>18</b> , 1587-1593 (2008).	cional
430 18. X. Li <i>et al.</i> , Mutually inhibitory Ras-PI(3,4)P2 feedback loops mediate cell migration. <i>Proc N</i>	atl
431 Acad Sci U S A <b>115</b> , E9125-E9134 (2018).	
432 19. Y. Miao <i>et al.</i> , Altering the threshold of an excitable signal transduction network changes c	ell
433 migratory modes. <i>Nat Cell Biol</i> <b>19</b> , 329-340 (2017).	
434 20. A. T. Sasaki, C. Chun, K. Takeda, R. A. Firtel, Localized Ras signaling at the leading edge regu	lates
435 PI3K, cell polarity, and directional cell movement. <i>The Journal of cell biology</i> <b>167</b> , 505-518	
436 (2004).	
437 21. S. Suire <i>et al.</i> , GPCR activation of Ras and PI3Kc in neutrophils depends on PLCb2/b3 and th	ie
438 RasGEF RasGRP4. <i>The EMBO journal</i> <b>31</b> , 3118-3129 (2012).	
439 22. M. J. Wang, Y. Artemenko, W. J. Cai, P. A. Iglesias, P. N. Devreotes, The directional respons	e of
440 chemotactic cells depends on a balance between cytoskeletal architecture and the externa	l
441 gradient. <i>Cell Rep</i> <b>9</b> , 1110-1121 (2014).	
442 23. L. Zheng, J. Eckerdal, I. Dimitrijevic, T. Andersson, Chemotactic peptide-induced activation	of Ras
443 in human neutrophils is associated with inhibition of p120-GAP activity. <i>The Journal of biol</i>	ogical
444 chemistry <b>272</b> , 23448-23454 (1997).	
445 24. P. J. van Haastert, I. Keizer-Gunnink, A. Kortholt, Coupled excitable Ras and F-actin activation	วท
446 mediates spontaneous pseudopod formation and directed cell movement. <i>Molecular biolo</i>	gy of
447 <i>the cell</i> <b>28</b> , 922-934 (2017).	
448 25. R. H. Insall, J. Borleis, P. N. Devreotes, The aimless RasGEF is required for processing of	
449 chemotactic signals through G-protein-coupled receptors in Dictyostelium. <i>Current biology</i>	: CB
450 <b>6</b> , 719-729 (1996).	
451 26. X. Xu, M. Meier-Schellersheim, X. Jiao, L. E. Nelson, T. Jin, Quantitative imaging of single liv	
452 reveals spatiotemporal dynamics of multistep signaling events of chemoattractant gradien	Ċ
453 sensing in Dictyostelium. <i>Molecular biology of the cell</i> <b>16</b> , 676-688 (2005).	_
454 27. X. Xu <i>et al.</i> , Quantitative Monitoring Spatiotemporal Activation of Ras and PKD1 Using Con	focal
455 Fluorescent Microscopy. <i>Methods Mol Biol</i> <b>1407</b> , 307-323 (2016).	
456 28. H. Kae, C. J. Lim, G. B. Spiegelman, G. Weeks, Chemoattractant-induced Ras activation duri	ng
457 Dictyostelium aggregation. <i>EMBO Rep</i> <b>5</b> , 602-606 (2004).	

**20 |** Page

458	29.	S. Suire <i>et al.</i> , Gbetagammas and the Ras binding domain of p110gamma are both important
459	25.	regulators of PI(3)Kgamma signalling in neutrophils. <i>Nat Cell Biol</i> <b>8</b> , 1303-1309 (2006).
460	30.	C. Knall <i>et al.</i> , Interleukin-8 regulation of the Ras/Raf/mitogen-activated protein kinase pathway
461		in human neutrophils. <i>The Journal of biological chemistry</i> <b>271</b> , 2832-2838 (1996).
462	31.	S. Yarwood, D. Bouyoucef-Cherchalli, P. J. Cullen, S. Kupzig, The GAP1 family of GTPase-
463	• = .	activating proteins: spatial and temporal regulators of small GTPase signalling. <i>Biochemical</i>
464		Society transactions <b>34</b> , 846-850 (2006).
465	32.	T. Grewal, M. Koese, F. Tebar, C. Enrich, Differential Regulation of RasGAPs in Cancer. <i>Genes</i>
466	•=-	Cancer <b>2</b> , 288-297 (2011).
467	33.	P. J. Lockyer, S. Kupzig, P. J. Cullen, CAPRI regulates Ca(2+)-dependent inactivation of the Ras-
468	55.	MAPK pathway. <i>Current biology : CB</i> <b>11</b> , 981-986 (2001).
469	34.	P. J. Lockyer <i>et al.</i> , Identification of the ras GTPase-activating protein GAP1(m) as a
470	51.	phosphatidylinositol-3,4,5-trisphosphate-binding protein in vivo. <i>Current biology : CB</i> <b>9</b> , 265-268
471		(1999).
472	35.	J. Zhang, J. Guo, I. Dzhagalov, Y. W. He, An essential function for the calcium-promoted Ras
473	55.	inactivator in Fcgamma receptor-mediated phagocytosis. <i>Nature immunology</i> <b>6</b> , 911-919 (2005).
474	36.	X. Xu <i>et al.</i> , GPCR-Mediated PLCbetagamma/PKCbeta/PKD Signaling Pathway Regulates the
475	50.	Cofilin Phosphatase Slingshot 2 in Neutrophil Chemotaxis. <i>Molecular biology of the cell</i>
476		10.1091/mbc.E14-05-0982 (2015).
477	37.	E. Rincon, B. L. Rocha-Gregg, S. R. Collins, A map of gene expression in neutrophil-like cell lines.
478	57.	BMC Genomics <b>19</b> , 573 (2018).
479	38.	M. Upadhyaya <i>et al.</i> , Mutational and functional analysis of the neurofibromatosis type 1 (NF1)
480	50.	gene. Hum Genet <b>99</b> , 88-92 (1997).
481	39.	Q. Liu <i>et al.</i> , CAPRI and RASAL impose different modes of information processing on Ras due to
482	55.	contrasting temporal filtering of Ca2+. <i>The Journal of cell biology</i> <b>170</b> , 183-190 (2005).
483	40.	I. R. Vetter, A. Wittinghofer, The guanine nucleotide-binding switch in three dimensions. <i>Science</i>
484		<b>294</b> , 1299-1304 (2001).
485	41.	K. Scheffzek, A. Lautwein, W. Kabsch, M. R. Ahmadian, A. Wittinghofer, Crystal structure of the
486		GTPase-activating domain of human p120GAP and implications for the interaction with Ras.
487		Nature <b>384</b> , 591-596 (1996).
488	42.	X. Xu, P. Johnson, S. C. Mueller, Breast cancer cell movement: imaging invadopodia by TIRF and
489		IRM microscopy. <i>Methods Mol Biol</i> <b>571</b> , 209-225 (2009).
490	43.	Z. Li <i>et al.</i> , Roles of PLC-beta2 and -beta3 and PI3Kgamma in chemoattractant-mediated signal
491		transduction. Science <b>287</b> , 1046-1049 (2000).
492	44.	G. Servant <i>et al.</i> , Polarization of chemoattractant receptor signaling during neutrophil
493		chemotaxis. Science <b>287</b> , 1037-1040 (2000).
494	45.	W. Tang <i>et al.</i> , A PLCbeta/PI3Kgamma-GSK3 signaling pathway regulates cofilin phosphatase
495		slingshot2 and neutrophil polarization and chemotaxis. <i>Dev Cell</i> <b>21</b> , 1038-1050 (2011).
496	46.	H. Cai <i>et al.</i> , Ras-mediated activation of the TORC2-PKB pathway is critical for chemotaxis. <i>The</i>
497		Journal of cell biology <b>190</b> , 233-245 (2010).
498	47.	D. D. Sarbassov, D. A. Guertin, S. M. Ali, D. M. Sabatini, Phosphorylation and regulation of
499		Akt/PKB by the rictor-mTOR complex. <i>Science</i> <b>307</b> , 1098-1101 (2005).
500	48.	D. R. Alessi <i>et al.</i> , Mechanism of activation of protein kinase B by insulin and IGF-1. <i>The EMBO</i>
501		journal <b>15</b> , 6541-6551 (1996).
502	49.	K. Mizuno, Signaling mechanisms and functional roles of cofilin phosphorylation and
503		dephosphorylation. <i>Cell Signal</i> <b>25</b> , 457-469 (2013).

504	50	
504	50.	H. Kitayama, Y. Sugimoto, T. Matsuzaki, Y. Ikawa, M. Noda, A ras-related gene with
505	54	transformation suppressor activity. <i>Cell</i> <b>56</b> , 77-84 (1989).
506	51.	J. L. Bos, All in the family? New insights and questions regarding interconnectivity of Ras, Rap1
507	5.2	and Ral. <i>The EMBO journal</i> <b>17</b> , 6776-6782 (1998).
508	52.	T. G. Bivona <i>et al.</i> , Rap1 up-regulation and activation on plasma membrane regulates T cell
509	5.2	adhesion. <i>The Journal of cell biology</i> <b>164</b> , 461-470 (2004).
510	53.	T. J. Jeon, D. J. Lee, S. Merlot, G. Weeks, R. A. Firtel, Rap1 controls cell adhesion and cell motility
511	<b>F</b> 4	through the regulation of myosin II. <i>The Journal of cell biology</i> <b>176</b> , 1021-1033 (2007).
512	54.	Y. Dai <i>et al.</i> , Ca2+-dependent monomer and dimer formation switches CAPRI Protein between
513		Ras GTPase-activating protein (GAP) and RapGAP activities. <i>The Journal of biological chemistry</i>
514		<b>286</b> , 19905-19916 (2011).
515	55.	J. Yi, X. S. Wu, T. Crites, J. A. Hammer, 3rd, Actin retrograde flow and actomyosin II arc
516		contraction drive receptor cluster dynamics at the immunological synapse in Jurkat T cells.
517	ГC	Molecular biology of the cell <b>23</b> , 834-852 (2012).
518	56.	X. Wen, T. Jin, X. Xu, Imaging G Protein-coupled Receptor-mediated Chemotaxis and its Signaling
519		Events in Neutrophil-like HL60 Cells. <i>J Vis Exp</i> 10.3791/54511 (2016).
520	57.	P. J. Lockyer <i>et al.</i> , Distinct subcellular localisations of the putative inositol 1,3,4,5-
521		tetrakisphosphate receptors GAP1IP4BP and GAP1m result from the GAP1IP4BP PH domain
522	ГQ	directing plasma membrane targeting. <i>Current biology : CB</i> <b>7</b> , 1007-1010 (1997).
523	58.	G. E. Cozier <i>et al.</i> , GAP1IP4BP contains a novel group I pleckstrin homology domain that directs
524		constitutive plasma membrane association. <i>The Journal of biological chemistry</i> <b>275</b> , 28261-
525	FO	28268 (2000).
526	59.	J. S. Parkinson, G. L. Hazelbauer, J. J. Falke, Signaling and sensory adaptation in Escherichia coli chemoreceptors: 2015 update. <i>Trends Microbiol</i> <b>23</b> , 257-266 (2015).
527 528	60.	S. L. Porter, G. H. Wadhams, J. P. Armitage, Signal processing in complex chemotaxis pathways.
528 529	60.	
529	61.	Nat Rev Microbiol <b>9</b> , 153-165 (2011). C. H. Hansen, R. G. Endres, N. S. Wingreen, Chemotaxis in Escherichia coli: a molecular model for
531	01.	robust precise adaptation. <i>PLoS Comput Biol</i> <b>4</b> , e1 (2008).
531	62.	B. A. Mello, Y. Tu, Effects of adaptation in maintaining high sensitivity over a wide range of
532	02.	backgrounds for Escherichia coli chemotaxis. <i>Biophys J</i> <b>92</b> , 2329-2337 (2007).
534	63.	D. Clausznitzer, O. Oleksiuk, L. Lovdok, V. Sourjik, R. G. Endres, Chemotactic response and
535	03.	adaptation dynamics in Escherichia coli. <i>PLoS Comput Biol</i> <b>6</b> , e1000784 (2010).
536	64.	Y. Xiong, C. H. Huang, P. A. Iglesias, P. N. Devreotes, Cells navigate with a local-excitation, global-
537	04.	inhibition-biased excitable network. <i>Proc Natl Acad Sci U S A</i> <b>107</b> , 17079-17086 (2010).
538	65.	M. Meier-Schellersheim <i>et al.</i> , Key role of local regulation in chemosensing revealed by a new
539	05.	molecular interaction-based modeling method. <i>PLoS Comput Biol</i> <b>2</b> , e82 (2006).
540	66.	T. Skorski <i>et al.</i> , p120 GAP requirement in normal and malignant human hematopoiesis. <i>J Exp</i>
541	00.	Med 178, 1923-1933 (1993).
542	67.	T. Grewal, C. Enrich, Molecular mechanisms involved in Ras inactivation: the annexin A6-
543	07.	p120GAP complex. <i>Bioessays</i> <b>28</b> , 1211-1220 (2006).
544	68.	T. Grewal <i>et al.</i> , Annexin A6-A multifunctional scaffold in cell motility. <i>Cell Adh Migr</i> <b>11</b> , 288-304
545	00.	(2017).
5.5		

# 546

# 547 Figure legends

548 **Fig. 1.** CAPRI interacts with Ras and regulates chemoattractant GPCR-induced Ras adaptation.

549 (A) fMLP-stimulated association between Ras/Rap1/Rac1 and CAPRI detected by co-

550 immunoprecipitation assay. (B) Expression of *capri* in HL60 cells transfected with non-specific

551 (CTL) or *capri* specific (*capri*<sup>kd</sup>) shRNA virus particles. CAPRI was detected by antibodies

against human CAPRI. Actin was detected as a loading control; fMLP receptor 1 FPR1 was also

detected in both CTL and *capri<sup>kd</sup>* cells. (C) fMLP-induced Ras activation in CTL and *capri<sup>kd</sup>* 

cells determined by a pull-down assay. Upon stimulation with 10  $\mu$ M fMLP at time 0", cells

were collected, lysed at the indicated time points, and then centrifuged at 10,000 g for 10 min at

556 4 °C. Agarose beads pre-conjugated with RBD-GST (active Ras binding domain of Raf1 tagged

with GST) were incubated with the supernatants of the lysates for 2 hours at 4 °C, then washed

with lysis buffer. The protein bound to agarose beads was eluted with 2X SDS loading buffer

559 (SLB). Aliquots of cells at the indicated time points were also mixed with the same volume of

560 SLB for the detection of total Ras protein. The elutes of RBD-GST beads and the aliquots of the

cells were analyzed by immunoblotting with anti-pan Ras antibody to detect either active Ras or

total Ras protein. (D) Normalized quantitative densitometry of the active Ras from three

independent experiments, including the result presented in C. The intensity ratio of active Ras

and total Ras in WT at time 0 s was normalized to 1. Mean  $\pm$  SD from three independent

565 experiments is shown. (E) Ras activation in CTL, *capri<sup>kd</sup>*, and *capri<sup>kd/OE</sup>* cells monitored by the

566 membrane translocation of the mRFP-tagged active Ras binding domain of Raf1 (RBD-RFP) in

<sup>567</sup> response to 1 μM fMLP stimulation. CTL (top panel and Video S1) and *capri<sup>kd</sup>* (middle panel

and Video S2) cells expressed RBD-RFP (red) and a plasma membrane maker (PM, green). The

569  $capri^{kd/OE}$  cell (bottom panel and Video S3) is a  $capri^{kd}$  cell expressing a PM marker (cyan),

# 570 CAPRI tagged with turboGFP (CAPRI-tGFP, green), and RBD-RFP (red). fMLP was applied to 23 | P a g e

571	the cells after 0 s. Scale bar, 10 $\mu$ m. (F) The quantitative measurement of Ras activation as the
572	membrane translocation of RBD-RFP in E is shown. Mean $\pm$ SD is shown; n = 3, 4, and 4 for
573	CTL, $capri^{kd}$ , and $capri^{kd/OE}$ cells, respectively.

Fig. 2. Chemoattractant-induced membrane targeting of CAPRI. (A) Colocalization of active Ras 574 and Rac1 with CAPRI in the leading edge of a chemotaxing cell. HL60 cells expressed a PM 575 marker (cyan), both tGFP-tagged CAPRI (green), and RBD-RFP (red) or actin-mCherry (red) 576 were exposed to a 100 nM fMLP gradient (dark blue). To visualize the fMLP gradient, 100 nM 577 578 fMLP was mixed with Alexa 633 (dark blue). Scale bar = 10  $\mu$ m. (B) The scheme shows the domain composition of tGFP-tagged wild-type (WT) or mutants of CAPRI. (C) Domain 579 580 requirement for the interaction of CAPRI and Ras determined by co-immunoprecipitation. HL60 cells expressing either tGFP alone or tGFP-tagged WT or mutants of CAPRI were lysed with 581 immunoprecipitation buffer with 1 mM GTPyS and went through the coimmunoprecipitation 582 process and western blotting using anti-GFP or Ras antibodies. (D) Montage shows the 583 membrane translocation of CAPRI and its mutants upon uniform application of 1 µM fMLP. 584 Cells expressing tGFP-tagged WT or mutants of CAPRI (green) and PM marker (red) were 585 586 imaged in time-lapse and 100 nM fMLP (red) was applied to the cells after 0 s. Scale bar = 10587 µm. Videos S4-S7 are CTL cells expressing PM marker (red) and tGFP-tagged WT, R472A,  $\Delta$ PH or  $\Delta$ C2 of CAPRI (green), respectively. (E) The quantitative measurement of the 588 membrane translocation of CAPRI or its mutants is shown. Mean  $\pm$  SD is shown, n = 5, 4, 4, and 589 590 4 for WT,  $\Delta C2$ ,  $\Delta PH$ , or R472A of CAPRI, respectively. The quantitative measurement of 591 intensity changes was described in the Materials and Methods section.

592	Fig. 3. Enhanced chemoattractant-induced activation of PI <sub>3</sub> K signaling in <i>capri<sup>kd</sup></i> cells. (A)
593	Montage shows the membrane translocation of PIP <sub>3</sub> biosensor PH-GFP in CTL and <i>capri<sup>kd</sup></i> cells
594	in response to 1 $\mu$ M fMLP stimulation. Cells expressing PH-GFP (GFP-tagged PH domain of
595	human AKT, green) and PM marker (red) were stimulated with 1 $\mu$ M fMLP at time 0 s. Scale
596	bar = 10 $\mu$ m. Videos S8 and S9 are CTL and <i>capri<sup>kd</sup></i> cells, respectively. (B) fMLP-induced
597	phosphorylation of AKT in CTL and <i>capri<sup>kd</sup></i> cells. A final concentration of 10 $\mu$ M fMLP
598	stimulation was added to the cells at time 0 s. Aliquots of cells were sampled at the indicated
599	time points and subjected to western blot detection of the phosphorylated and total proteins of
600	interest in A and C. (C) Normalized quantitative densitometry of phosphorylated AKT by total
601	AKT protein in <b>B</b> . Mean $\pm$ SD of three independent experiments is shown. The intensity ratio of
602	the phosphorylated versus total AKT in CTL cells at time 0 s is normalized to 1. (D) fMLP-
603	induced phosphorylation of GSK3 $\alpha/3\beta$ and cofilin in CTL and <i>capri<sup>kd</sup></i> cells. (E) Normalized
604	quantitative densitometry of the phosphorylated GSK3 $\alpha/3\beta$ , and cofilin in <b>D</b> . The intensity ratio
605	of the phosphorylated versus total GSK3 $\alpha/\beta$ and cofilin in CTL cells at time 0 s is normalized to
606	1. Mean $\pm$ SD of three independent experiments is shown.
607	Fig. 4. Increased activation of Rap1 and its effector induced by fMLP stimulation in <i>caprikd</i>

608 cells. (A) fMLP-induced Rap1 activation in CTL and  $capri^{kd}$  cells determined by a pull-down

assay using GST-RBD<sub>RalGDS</sub> agarose beads. (B) Normalized quantitative densitometry of the

active Rap1 from three independent experiments, including the result presented in A. The

- intensity ratio of active Rap1 and total Rap1 in WT at time 0 s was normalized to 1. Mean  $\pm$  SD
- from three independent experiments is shown. (C) fMLP-induced Rap1 activation monitored by
- 613 the membrane translocation of the active Rap1 probe GFP-RBD<sub>RalGSD</sub>. Cells expressing

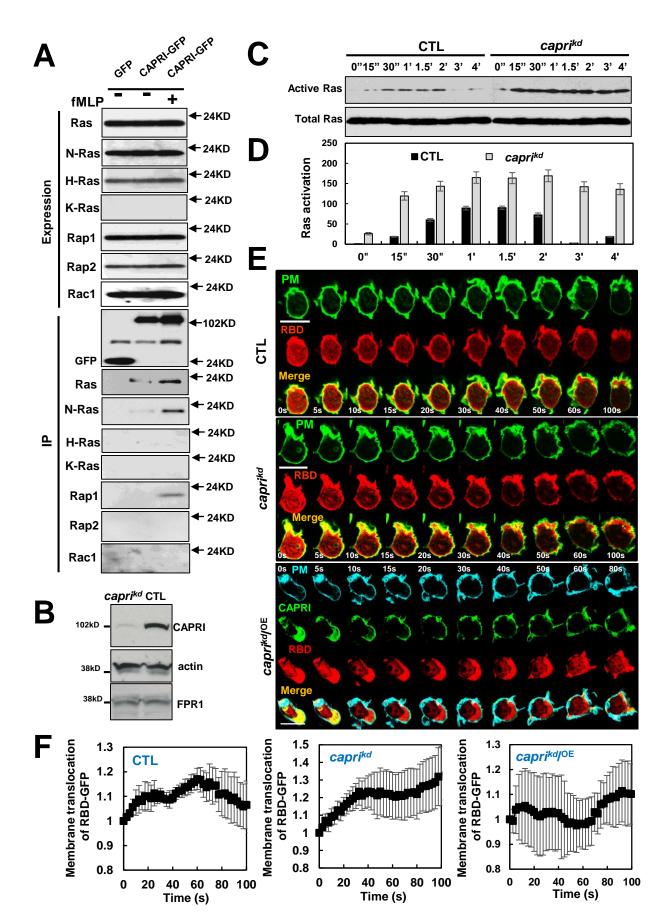
614	$RBD_{RalGSD}$ -GFP (green) and PM marker (red) were stimulated with 1 $\mu$ M fMLP at 0 s. Scale bar
615	= 10 $\mu$ m. Videos S11-S12 are CTL and <i>capri<sup>kd</sup></i> cells, respectively. (D) fMLP-induced
616	phosphorylation of Erk42/44 in CTL and <i>caprikd</i> cells. (E) Normalized quantitative densitometry
617	of the phosphorylated Erk42/44 in E. The intensity ratio of the phosphorylated versus total
618	Erk42/44 in CTL cells at time 0 s is normalized to 1. Mean $\pm$ SD of three independent
619	experiments is shown.
620	Fig. 5. Elevated polymerization of actin in response to a high concentration of fMLP stimulation
621	impairs the polarity and migration of <i>capri<sup>kd</sup></i> cells. (A) The amount of globular (G) and
622	filamentous (F) actin in CTL and <i>caprikd</i> cells was determined by a centrifugation assay of F-
623	actin. Cells were stimulated with 10 $\mu$ M fMLP at time 0 s and aliquots of cells at the indicated
624	time points were analyzed. (B) Normalized quantitative densitometry of the F/G-actin ratio in the
625	CTL and of $capri^{kd}$ cells in (A). Mean $\pm$ SD from three independent experiments is shown. The
626	F/G ratio of CTL cells at 0 s was normalized to 1. (C) fMLP-induced actin polymerization by
627	monitoring F-actin probe GFP-F-tractin using live cell confocal microscopy in CTL and <i>caprikd</i>
628	cells. Cells expressing tractin-GFP (green) and PM marker (red) were stimulated with 1 $\mu M$
629	fMLP at time 0 s. Scale bar = 10 $\mu$ m. Videos S12-S13 are CTL and <i>capri<sup>kd</sup></i> cells, respectively.
630	(D) F-actin distribution in chemotaxing CTL and <i>capri<sup>kd</sup></i> cells in a 1 $\mu$ M fMLP gradient. The
631	differentiated cells were stained with the actin filament probe, SiR-actin (red). Cells were
632	exposed to a 1 $\mu$ M fMLP gradient and allowed to chemotax for 5 min. Arrows point to the cells
633	with a polarized, chemotaxing morphology. To visualize the gradient, fMLP was mixed with
634	Alexa 488 (green, 1 $\mu$ g/ml). Scale bar = 20 $\mu$ m. Videos S14-S15 are CTL and <i>capri<sup>kd</sup></i> cells,

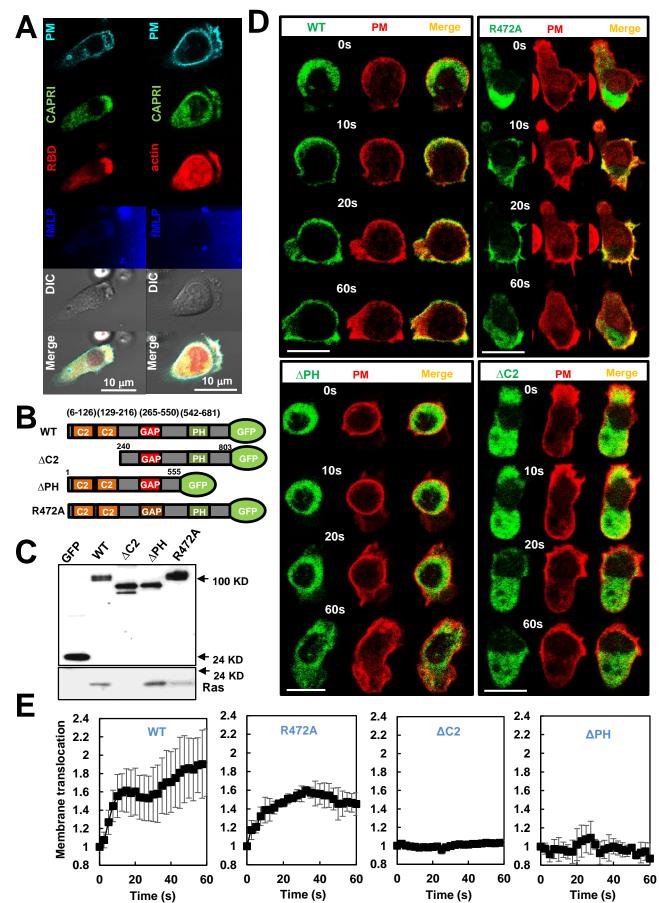
respectively. (E) The graph shows the roundness of CTL and  $capri^{kd}$  cells shown in **D**. The

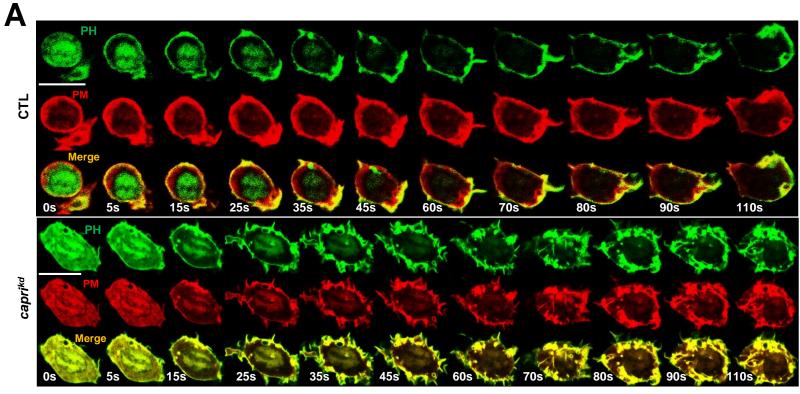
636	roundness was measured as the ratio of the width vs the length of the cell. That is, the roundness
637	for a circle is 1 and for a line is 0. Student's <i>t</i> -test was used to calculate the <i>p</i> value.

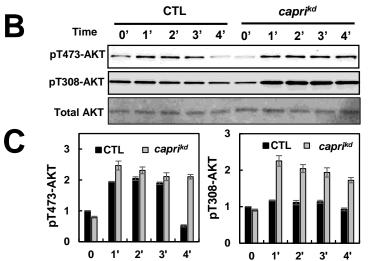
638	Fig. 6. The concentration range of fMLP gradients in which neutrophils chemotax efficiently is
639	upshifted in <i>capri<sup>kd</sup></i> cells. (A) Montages showing the travel path of chemotaxing CTL or <i>capri<sup>kd</sup></i>
640	cells in a gradient generated from a 1 $\mu$ M fMLP source. Cell movement was analyzed by DIAS
641	software. (B) Chemotaxis behaviors measured from A are described as four parameters:
642	directionality, which is "upward" directionality, where 0 represents random movement and 1
643	represents straight movement toward the gradient; speed, defined as the distance that the centroid
644	of the cell moves as a function of time; total path length, the total distance the cell has traveled;
645	and roundness (%) for polarization, which is calculated as the ratio of the width to the length of
646	the cell. Thus, a circle (no polarization) is 1 and a line (perfect polarization) is 0. Thirteen cells
647	from each group were measured and the mean $\pm$ SD was shown. Student's <i>t</i> -test was used to
648	calculate the p value. (C) Montages show the travel path of chemotaxing CTL or $capri^{kd}$ cells in
649	response to a wide range of fMLP gradients. (D) Chemotaxis behaviors measured from C are
650	described by three parameters: directionality, speed, and total path length as described in <b>B</b> .
651	Thirteen cells from each group were measured. Student's $t$ -test was used to calculate the $p$ value.
652	Fig. 7. Activity of Ras and Rap1 is increased in <i>capri<sup>kd</sup></i> cells. (A) CAPRI localizes at the plasma
653	membrane before and after fMLP stimulation. (B) Ras and Rap1 activation in CTL and <i>caprikd</i>
654	cells in response to 0.1 nM, 10 nM, or 1 $\mu$ M fMLP stimulation determined by a pull-down assay.
655	(C) Normalized quantitative densitometry of the active Ras and Rap1 from three independent
656	experiments, including the result presented in <b>B</b> . The intensity ratio of active Ras and Rap1 in
657	WT at time 0 s was normalized to 1. Mean $\pm$ SD from three independent experiments is shown.

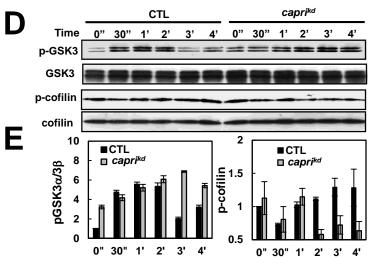
658	Fig. 8. <i>capri<sup>kd</sup></i> cells are more sensitive to the stimuli at low concentration and fail to adapt to the
659	stimuli at high concentrations. (A) Montage shows cell response as actin polymerization
660	monitored through the membrane translocation of F-actin probe, Ftractin-GFP, in both CTL or
661	<i>capri</i> <sup>kd</sup> HL60 cells using fluorescent microscopy. Cells expressing GFP-F-tractin (green) and PM
662	marker (red) were stimulated with either 0.1 nM or 10 nM fMLP stimulation. Scale bar = $10 \ \mu m$ .
663	Videos S16 and S18 are CTL cells and Videos S17 and S19 are <i>capri<sup>kd</sup></i> cells. Videos S16-S17
664	and Videos S18-19 were cells stimulated with either 0.1 nM or 10 nM fMLP, respectively. (B)
665	The percentage of cells that respond to the indicated concentration of fMLP stimuli in CTL and
666	<i>capri</i> <sup>kd</sup> cells is shown. (C) Percentage of cells with adaptation in response to fMLP stimulation.
667	<b>B</b> and <b>C</b> were measured with the same sets of data. The numbers of independent experiments for
668	CTL and <i>capri<sup>kd</sup></i> cells for 0.1 nM, 10 nM, and 1 $\mu$ M fMLP stimuli are 11 and 7, 8 and 10, and 5
669	and 9, respectively. Student's <i>t</i> -test was used to calculate the <i>p</i> value.

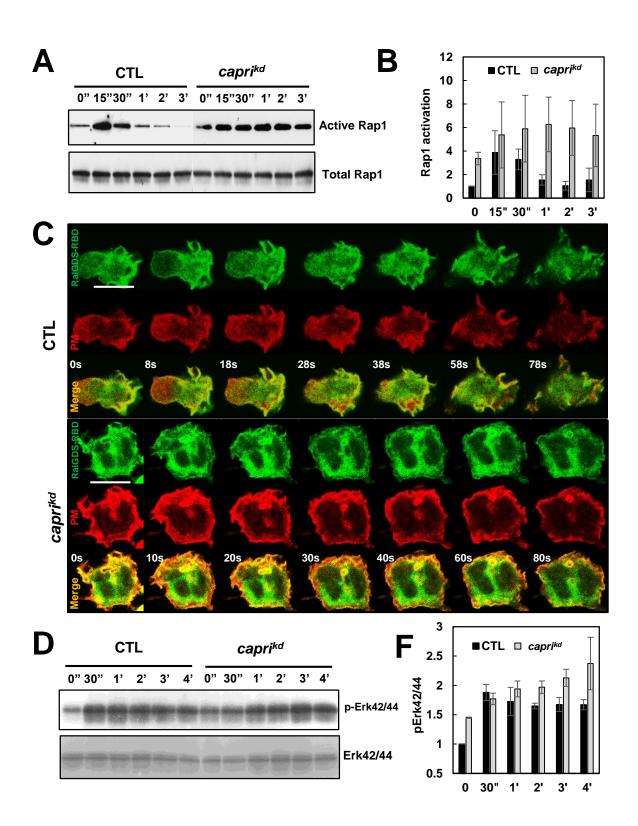


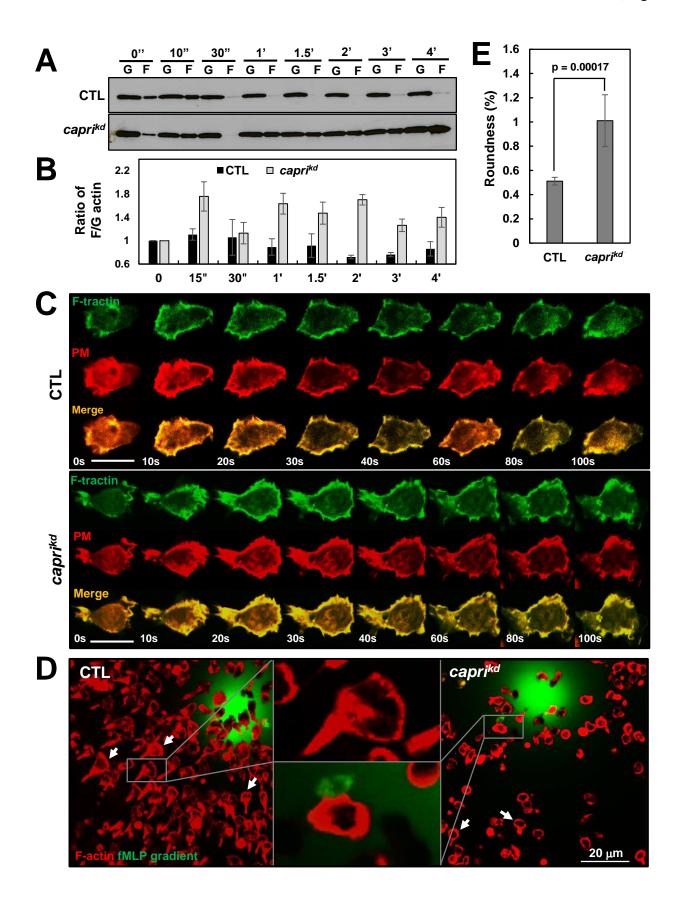












Xu et al., Figure 6

